JACS
JOURNAL OF THE AMERICAN CHEMICAL SOCIETY

Article

pubs.acs.org/JACS

DNA-Mediated Signaling by Proteins with 4Fe−4S Clusters Is Necessary for Genomic Integrity

Michael A. Grodick, Helen M. Segal, Theodore J. Zwang, and Jacqueline K. Barton*

Division of Chemistry and Chemical Engineering, California Institute of Technology, Pasadena, California 91125, United States

Supporting Information

ABSTRACT: Iron−sulfur clusters have increasingly been found to be associated with enzymes involved in DNA processing. Here we describe a role for these redox clusters in DNA-mediated charge-transport signaling in *E. coli* between DNA repair proteins from distinct pathways. DNA-modified electrochemistry shows that the 4Fe−4S cluster of DNA-bound DinG, an ATP-dependent helicase that repairs R-loops, is redox-active at cellular potentials and ATP hydrolysis increases DNA-mediated redox signaling. Atomic force microscopy experiments demonstrate that DinG and Endonuclease III (EndoIII), a base excision repair enzyme, cooperate at long-range using DNA charge transport to redistribute to regions of DNA damage. Genetics experiments, moreover, reveal that this DNA-mediated signaling among proteins also occurs within the cell and, remarkably, is required for cellular viability under conditions of stress. Silencing the gene encoding EndoIII in a strain of *E. coli* where repair by DinG is essential results in a significant growth defect that is rescued by complementation with EndoIII but not with an EndoIII mutant that is enzymatically active but unable to carry out DNA charge transport. This work thus elucidates a fundamental mechanism to coordinate the activities of DNA repair enzymes across the genome.

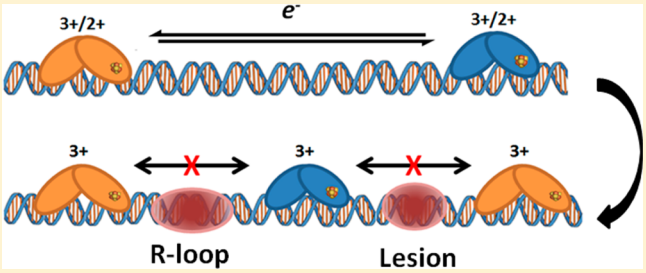

INTRODUCTION

Iron−sulfur clusters are increasingly being found in proteins that are tasked with maintaining the fidelity of the genome.[1−3] These clusters were first observed in DNA-binding proteins in the base excision repair (BER) glycosylase, Endonuclease III (EndoIII).[4] More recently, 4Fe−4S clusters have been found in a range of DNA repair and DNA processing enzymes including helicases, DNA and RNA polymerases, DNA helicase-nucleases, and DNA primases from across the phylogeny.[2,4−13] Many of the enzymes that have been shown to contain these clusters are genetically linked to human diseases, such as early onset breast cancer and Fanconi's anemia, yet the proteins perform immensely different functions. The clusters do not participate in catalysis in these proteins,[2,3,5] though DNA binding may be affected by perturbing the cluster.[14] Recently, studies focusing on the biogenesis of iron−sulfur clusters have revealed that disruption of iron−sulfur cluster assembly proteins in eukaryotic cells leads to nuclear genomic instability and defects in DNA metabolism, replication, and repair.[15−17] The ubiquity of these complex cofactors suggests an essential and shared role for their presence in DNA processing enzymes.

We have considered that the 4Fe−4S clusters in DNA repair enzymes may serve as redox cofactors, much as 4Fe−4S clusters do in other enzymes within the cell.[1,18] Most of our work has focused on *E. coli* EndoIII, where the 4Fe−4S cluster was first found. Although a redox role for the cluster was considered,[4] the 4Fe−4S cluster in EndoIII is redox-inactive at typical cellular potentials. We showed, however, that DNA binding shifts the redox potential of the cluster to 80 mV vs the normal hydrogen electrode (NHE), moving the 3+/2+ redox couple into the physiological regime.[19] Strikingly, we have now seen that 4Fe−4S clusters in other repair proteins share this DNA-bound potential of ∼80 mV versus NHE.[20,21] We have proposed that these clusters are utilized for DNA-mediated charge-transport (CT) chemistry as a first step in the search for DNA lesions to repair.[18,22] Indeed we have explored how EndoIII and another BER glycosylase with a 4Fe−4S cluster, MutY, may use DNA CT cooperatively as a first step in repair.[22] Here we explore how DNA CT may be utilized more generally in *E. coli* for interprotein signaling between repair pathways to maintain the integrity of the genome.

The chemistry of DNA CT offers a powerful tool to probe the integrity of duplex DNA. It has now been well documented that DNA can conduct charge through the π-stacked base pairs within the helix.[23] Subtle perturbations to the DNA base stack, including the presence of base pair mismatches, abasic sites, or even DNA lesions, such as those that are substrates for DNA glycosylases, attenuate DNA CT.[18,24] Protein binding can also interrupt DNA CT if it disrupts base stacking, as seen with enzymes that flip DNA bases out of the helix.[25] This CT chemistry has been used to develop electrochemical sensors that detect base lesions, mismatches, and DNA-binding proteins on DNA-modified electrodes.[18,25−27] Charge can be transported through DNA over long molecular distances, and

Received: February 25, 2014
Published: April 16, 2014

   dx.doi.org/10.1021/ja501973c | *J. Am. Chem. Soc.* 2014, 136, 6470−6478

the distance dependence of CT is quite shallow.[23] In fact, charge can be efficiently transported through at least 100 base pairs, and over this distance the rate is still limited by transport through the linker rather than the DNA base stack.[28,29] Given that DNA CT can occur over long molecular distances and can be modulated by DNA-binding proteins, does DNA-mediated CT play a general role within the cell?

Recently DinG, a DNA damage response helicase from *E. coli*, was shown to contain a 4Fe−4S cluster.[30] DinG is part of the SOS response, which is activated by DNA damaging agents and cellular stressors. DinG shares homology with the nucleotide excision repair protein XPD as well as with a host of Superfamily 2 helicases from archaea and eukaryotes that are linked to human disease and share a conserved 4Fe−4S domain.[5] DinG unwinds DNA that has single-stranded overhangs with a 5′ to 3′ polarity.[31] DNA−RNA hybrid duplexes that form within a DNA bubble, termed R-loops, represent a unique substrate that DinG has been shown to unwind *in vitro*.[32] Importantly, DinG is required to unwind R-loops *in vivo* in order to resolve stalled replication forks and thus to maintain the integrity of the genome.[33] Here we examine the DNA-bound redox properties of DinG and explore more generally crosstalk among redox-active DNA processing enzymes in *E. coli* via 4Fe−4S clusters.

EXPERIMENTAL METHODS

Expression and Purification of DinG. The *dinG* gene was amplified from *E. coli* and was inserted into a pET-28 b (+) vector (Novagen) as described previously.[30] After the vector was isolated, the cloned *dinG* gene was sequenced (Laragen) using the primers listed in Table S1. An aliquot of BL21(DE3) competent cells (Invitrogen) was then transformed with the pET28b-*dinG* vector. The constructed pET28b-*dinG* vector encodes for DinG with a C-terminal hexahistidine affinity tag.

To express DinG, 6 L of LB, which had been inoculated with an overnight culture of BL21(DE3) cells harboring the pET28b-*dinG* vector, was shaken at 37 °C. After the cultures reached an optical density of ∼0.6−0.8, enough IPTG (Research Products International Corp.) was added to bring the concentration of IPTG in each flask to 150 μM. The flasks were then returned to the incubator, which had been cooled to ∼22 °C. After ∼16 h of IPTG induction at ∼22 °C, the cells were collected by centrifugation at 5500 rpm for 15 min. The cell pellets were frozen at −80 °C.

To purify DinG, the cell pellets were resuspended in 300 mL buffer A (20 mM Tris-HCl, 8.0 pH at 4 °C, 0.5 M NaCl, and 20% glycerol) with added DNaseI from bovine pancreas (10 kU, Sigma) and complete protease inhibitor cocktail tablets (Roche). The cells were lysed using microfluidization. The lysate was centrifuged at 12 000 rpm for 45 min, and the supernatant from the cell lysate was filtered and loaded onto a 5 mL Histrap HP (GE healthcare) nickel-affinity column that had been equilibrated with buffer A. The column was then connected to an ÄKTA fast protein liquid chromatography (GE Healthcare) and was washed with 3−5 column volumes (CV) of buffer A. The protein was eluted using a linear gradient from 0 to 20% buffer B (20 mM Tris-HCl, 8.0 pH at 4 °C, 0.5 M NaCl, 500 mM imidazole, and 20% glycerol) over 10 CV, followed by a linear gradient from 20 to 30% buffer B over 10 CV. Fractions containing the desired protein, which were yellow and eluted at ∼150 mM imidazole, were desalted into buffer C using a Hiprep 26/10 desalting column (GE Healthcare). The collected protein was then concentrated down to 10−13 mL using an Amicon Ultra-15 centrifugal filter unit (Millipore) and was loaded onto a Hiload Superdex 200 26/600 pg (GE healthcare) that had been equilibrated with buffer C. The protein eluted after ∼180 mL of buffer C (20 mM Tris-HCl, 8.0 pH at 25 °C, 0.5 M NaCl, and 20% glycerol) had passed over the column. The purity of the protein was confirmed using SDS-PAGE (Figure S1). A helicase activity assay for DinG, modified from previously published procedures, was used to show that the protein is active after purification.[30,32]

DNA-Modified DinG Electrochemistry. The DNA substrate used for the electrochemical characterization of DinG was either a well-matched 20-mer DNA oligomer with a 15-mer 5′ to 3′ single-stranded overhang or the same substrate with the exception of an abasic site being placed on the complementary strand four base pairs from the bottom of the duplex (Table S1). A 20-mer strand of DNA with a terminal thiol and 6-carbon linker at the 5′ end of the strand was annealed to a 35-mer unmodified strand of DNA to yield the electrochemical substrate. The electrochemical substrate was designed to be competent to be unwound by DinG in a helicase reaction. Single-stranded DNA stimulates the ATPase activity of DinG, which requires at least a 15-mer single-stranded 5′ to 3′ overhang in order to unwind DNA substrates *in vitro*.[32] In the electrochemical cell, the DNA substrate is covalently tethered to the gold surface via a gold−thiol bond.

The thiol-modified strand was synthesized on a 3400 Applied Biosystems DNA synthesizer using standard phosphoramidite chemistry. The complementary strands were purchased from IDT. All phosphoramidites, including the terminal phosphoramidite containing a 6-carbon disulfide linker, were purchased from Glen Research. The thiol-modified and complementary strands were purified by HPLC using an analytical C-18 column (Agilent). DNA strands were characterized by MALDI mass spectroscopy. The DNA was quantified by UV−vis absorbance, and equimolar amounts were annealed yielding the duplex substrate.

To prepare DNA-modified single electrodes, a 50 μM solution of the DNA substrate was incubated overnight at ambient temperature on a bare gold on mica surface (Agilent) in an electrochemical cell with a capacity of 50 μL. Following incubation with the DNA solution, the surface was rinsed and backfilled by incubating the electrode with 1 mM 6-mercapto-1-hexanol for 45 min at room temperature. Multiplex chip electrodes were prepared as described previously.[29,34] The well-matched electrochemistry substrate was used for all single electrode experiments. For experiments with multiplex chip electrodes, the well-matched and abasic-site substrates were laid down side-by-side in separate quadrants on a single chip.[29,34]

After backfilling, the DNA-modified electrodes were rinsed with the electrochemistry buffer (4 mM spermidine, 4 mM $MgCl_2$, 0.25 mM EDTA, 20% glycerol, 250 mM NaCl, 20 mM Tris-HCl, pH ∼8.5). Protein concentration was measured by UV−vis absorbance using an extinction coefficient at 410 nm of 17 000 M^{-1} cm^{-1}.[22] An aliquot of 20 μM DinG was flash thawed by incubating it in a room temperature water bath. The protein's buffer was exchanged for the electrochemistry buffer by diluting the protein two-fold into 2× spermidine buffer (8 mM spermidine, 8 mM $MgCl_2$, 1 mM EDTA, 20 mM Tris-HCl, pH ∼9.0).

Electrochemical measurements were made using a CHI620D Electrochemical Analyzer. For cyclic voltammetry, sweeps within a window from −0.4 V vs Ag/AgCl to 0.1 or 0.2 V were carried out at a scan rate of 50 mV/s for several hours. For electrochemistry measurements on single electrodes with ATP, 1 mM ATP or 1 mM ATPγS (Sigma) was added after the electrochemical signal grew in to an appreciable size (>20 nA). Cyclic voltammetry was then used to scan the electrode over several hours.

Atomic Force Microscopy (AFM) Redistribution Assay. AFM experiments were performed using a protocol similar to that reported previously with the following modifications.[22,35] The long and short strands of DNA have an identical sequence as they were both amplified off of the pUC19 plasmid with primers containing a 2′ *O*-methyl residue to generate 1.8 and 2.2 kb strands of DNA with 14-mer single-stranded overhangs, so that the two could be subsequently ligated. For well-matched long strands of DNA, the two PCR products were annealed with complementary 14 bp overhangs. For the mismatched long strands of DNA, the strands were annealed in the same way except one of the PCR products contained a 14 bp overhang with a single base changed to yield a C:A mismatch upon the annealing of the two strands. Prior to deposition, the protein and DNA solution was incubated at 4 °C for 2 h. The sample was then deposited (5−10

μL) onto a freshly cleaved mica surface for 2 min, rinsed with 2 mL of water, and dried under argon. The concentration of DinG was 60 nM for AFM experiments with DinG. For AFM experiments with mixtures of DinG and EndoIII or DinG and EndoIII Y82A, the concentration of each protein was 30 nM.

Images of protein and DNA mixtures that had been deposited on dry mica surfaces were gathered using a Bruker Dimension Icon AFM (Beckman Institute MMRC). Images were captured in air with scan areas of 2 × 2 or 3 × 3 μm^2 in soft tapping mode and a scan rate of 3.00 Hz. RFESPA silicon AFM probes with reflective aluminum backing (Bruker), with a spring constant of 3 N/m and a resonance frequency of 69−81 kHz, were used for gathering images.

Bruker nanoscope analysis software was used to measure general DNA contour lengths and height profiles of the proteins. For each data set, images from at least three independently prepared surfaces were analyzed. At least 50 images were analyzed for both the mismatched DNA−protein samples and the well-matched samples. The binding density ratio, *r*, is defined as the ratio of the density of proteins bound on the long strands of DNA divided by the density of proteins bound on the short strands of DNA. The density of proteins on each strand is found by dividing the number of proteins by the length of the DNA strands, 3.8 kb pairs for the long strand and 1.9 kb pairs, which is the average length of the short strands, for short strands. Error represents SEM ($n \geq 3$) for each experiment. Distinguishable strands and bound proteins were counted by hand. In order to control for bias, for each experiment, images were randomly assigned identification numbers. The images were then scored blindly. The numbers of long strands, proteins on long strands, short strands, and proteins on short strands were collected for each image.

Binding density ratios can also be calculated for each individual image, which are treated as replicates, to obtain the average binding density ratio for each sample. The binding density ratios were plotted as a histogram (Figure S2), which show that the binding density ratios for the two sets of data follow a normal distribution around the mean, allowing for statistical analysis with a two-tailed *t* test. Binding density ratios obtained using this methodology are presented in the Supporting Information

MutY Activity Assay (CC104 *lac*$^+$ Forward Reversion Assay). The method used to inactivate *dinG* on the genome within the CC104 strain was adapted from a previously published procedure.[36] The FRT-flanked chloramphenicol acetyltransferase gene, *cat*, from pKD3 was amplified by PCR using the Δ*dinG*::cm^R forward primer and Δ*dinG*::cm^R reverse primer (Table S1). Following inactivation of *dinG* in the CC104 strain, colony PCR with the Δ*dinG*::cm^R forward and reverse sequencing primers (Table S1) was performed to confirm *dinG* had been replaced by *cat*. All PCR products were sequenced to confirm that the chromosomal gene disruption was successful (Laragen).

All mutant EndoIII plasmids, which were derived from pBBR1MCS-4,[37] were generated using a QuikChange II Site-Directed Mutagenesis kit (Agilent). The pBBR1MCS-4, pBBR1MCS-4-*nth*, pBBR1MCS-4-*nth* D138A, and pBBR1MCS-4-*nth* Y82A plasmids encode and constitutively express no protein, WT EndoIII, EndoIII D138A, and EndoIII Y82A, respectively. The pBBR1MCS-4 derived plasmids are referred to as p(empty), p(WT EndoIII), p(EndoIII D138A), and p(EndoIII Y82A), respectively, throughout the text as indicated in Table S2. The p(WT EndoIII) plasmid that was used as the template for the site-directed mutagenesis reactions was previously constructed in our laboratory.[35] The primers outlined in Table S1 were used to make the p(EndoIII Y82A) and p(EndoIII D138A) mutant plasmids. The isolated plasmids were sequenced (Laragen) using the forward and reverse pBBR1MCS-4-*nth* sequencing primers (Table S1) to verify that the desired mutation had been made in the *nth* gene.

The MutY activity assay was adapted from a previously published procedure.[22,38] The CC104 or CC104 Δ*dinG*::cm^R strains were transformed by electroporation with the p(EndoIII D138A), p(empty), and p(EndoIII Y82A) plasmids (Table S2). Following transformation, the cells were recovered in 1 mL LB for 2 h. The cells were spread on LB ampicillin (100 μg/mL) agar plates and incubated for 16 h, after which a single transformant was restreaked onto a fresh LB ampicillin (100 μg/mL) agar plate. These plates were incubated at 37 °C for 12 h.

One colony from each strain was used to inoculate a 1 mL LB ampicillin (100 μg/mL) culture. These cultures were incubated with shaking at 37 °C for 16 h. Next, 250 μL of each culture was spread onto NCE lactose (0.2% w/v) ampicillin (40 μg/mL) agar plates and incubated at 37 °C. The number of colony-forming units, representing *lac*$^+$ revertants, was counted after 48 h. Differences for growth between strains were monitored by evaluating the number of colony forming units on NCE glucose (0.2% w/v) ampicillin (40 μg/mL) agar plates. Note that we assay for MutY activity rather than EndoIII since the frequency of spontaneous GC:TA transversions associated with 8-oxoG:A repair by MutY is far greater than the pyrimidine lesions repaired by EndoIII.

InvA Δ*nth* Growth Assay. The genomic *nth* gene, encoding EndoIII, was knocked out of the InvA strain using P1 phage transduction.[39] The JW1625−1 *E. coli* strain from the Keio collection was used as a donor strain to transduce the *nth*::kan^R marker into an *E. coli* strain, BW16847, which is an *E. coli* MG1655 derivative that contains a Tn10 genomic marker near or within the *purR* gene, which is around 26 kb downstream of the *nth* gene (Table S3). Both the *nth*::kan^R and Tn10 markers from this newly generated strain (MG001 in Table S3) were transduced into the InvA strain, allowing for isolation of the *nth* knockout in InvA (InvA Δ*nth*) by selection on tetracycline LB agar plates followed by verification of the disruption using colony PCR with the *nth* genomic check primers (Table S1). Plasmids that constitutively express various mutants of EndoIII were prepared as outlined in the MutY activity assay section above. The EndoIII plasmids p(WT EndoIII), p(EndoIII D138A), p(EndoIII Y82A), and p(empty), in addition to an RNaseH overexpression plasmid (Table S2) designated p(RNaseH), were transformed into the InvA Δ*nth* strain using standard electroporation techniques. Colony PCR using the InvA check 1 and check 2 primers (Table S1) was used to verify that InvA-derived strains still contained the inverted *rrnA* operon after these genetic manipulations and transformations. Colony PCR with the genomic *nth* check primers (Table S1) was used to verify that the *nth* gene was knocked out of each putative Δ*nth* strain.

Growth curves of the InvA Δ*nth* strain in addition to InvA Δ*nth* transformed with p(WT EndoIII), p(EndoIII Y82A), p(EndoIII D138A), p(empty), or p(RNaseH) were used to assess the effect of knocking out the *nth* gene from the InvA background. Single colonies from LB ampicillin (100 μg/mL), or LB plates for each of the strains were used to inoculate separate cultures of LB, LB ampicillin (100 μg/mL), MM (M9 + 0.2% glucose),[40] or MM ampicillin (100 μg/mL). Cell growth was then monitored through measurement of the optical density at 600 nm for each of the cultures over time in LB or MM.

RESULTS

DNA Binding Activates DinG toward Reduction and Oxidation at Cellular Redox Potentials. DNA-modified electrodes were utilized to explore the DNA-bound redox chemistry of DinG. Cyclic voltammetry of the protein on gold electrodes modified with a 20-mer duplexed DNA oligomer appended with a 15-base 5′ single-stranded overhang displays a reversible redox potential for DinG of 80 mV vs NHE (Figure 1). This DNA-bound potential differs from the midpoint redox potential of ∼ −390 mV vs NHE assigned to the $[4Fe-4S]^{2+/1+}$ couple of the cluster observed in the absence of DNA as measured by titrations with redox mediators.[30] Cyclic voltammetry of DinG on multiplexed electrodes reveals that a single abasic site placed in the DNA duplex attenuates the current by 12 ± 3%, consistent with the signal being DNA mediated.[23,34] Moreover, upon addition of ATP to DinG bound to DNA-modified electrodes, the reductive and oxidative peak currents markedly increase; ATPγS, which is poorly hydrolyzed, does not yield a significant increase in current (Figure 1). Thus,

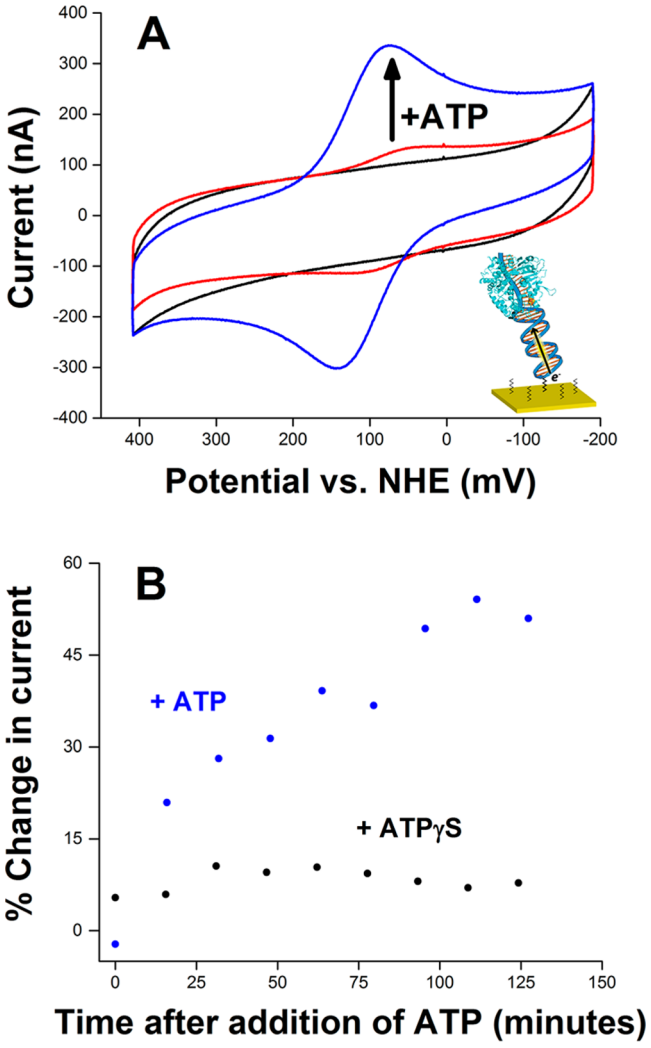

Figure 1. Electrochemistry of DinG on DNA-modified electrodes. (A) Cyclic voltammogram of 10 μM DinG (red), DinG after the addition of 5 mM ATP (blue), and buffer only (black) after incubation for 3 h. Inset: Cartoon representation of a protein bound to DNA on a DNA-modified electrode. (B) Percent change in current after the addition of 1 mM ATP (blue) or 1 mM ATPγs (black). Percent change in current is the percent increase in the measured current compared to the predicted current, based on the linear growth of the signal with respect to time for the incubation of DinG before the addition of ATP.

it appears that the ATPase activity of DinG can be monitored electrically, even though ATP hydrolysis is a redox-independent process. Similar results were seen earlier with *S. acidocaldarius* XPD (SaXPD), also an ATP-dependent helicase.[21] It is interesting to consider that this electronic signaling of activity may be used within a biological context.

EndoIII and DinG use DNA CT to Redistribute to Sites of DNA Damage. Given that DinG displays a DNA-bound potential similar to that of EndoIII of ~80 mV vs NHE, we sought to test whether EndoIII and DinG can signal to one another via DNA CT *in vitro* to aid one another in finding lesions that disrupt CT. It is noteworthy that both repair proteins are involved in finding lesions that interrupt DNA CT. Using AFM, we examined whether the DinG helicase would redistribute onto 3.8 kilobase (kb) DNA strands containing a single base mismatch, which interrupts DNA CT, rather than remaining bound to well-matched DNA strands. Our model for how repair proteins utilize DNA CT predicts such a redistribution as a first step in repair (*vide infra*), and this assay provides direct support for the model. If proteins of similar potential carry out DNA CT on well-matched DNA strands and dissociate from DNA upon reduction, they should preferentially redistribute onto DNA strands where DNA CT is inhibited by an intervening mismatch. Note that, while a single base mismatch inhibits DNA CT, it is not a substrate for either DinG or EndoIII binding. We have utilized this AFM assay previously to test EndoIII redistribution as a first step in finding damage.[22] We have also utilized this assay to test CT signaling between EndoIII and SaXPD, which also contains a 4Fe–4S cluster with a DNA-bound potential of ~80 mV vs NHE, in locating DNA damage;[21,35] these proteins are present in completely distinct organisms, but based on their shared DNA-bound potential are able to signal one another using DNA CT.

In this AFM assay, DNA–protein mixtures are deposited onto a dry mica surface on which single molecules of both free and protein-bound DNA can be visualized.[22,35] Duplexes of DNA that contain a single C:A mismatch located in the middle of the strand are mixed with fully matched DNA. These strands can be distinguished in the AFM by their difference in length: the mismatched strands are ~3.8 kb pairs long, while the matched strands on average contain ~1.9 kb pairs (Figure 2).

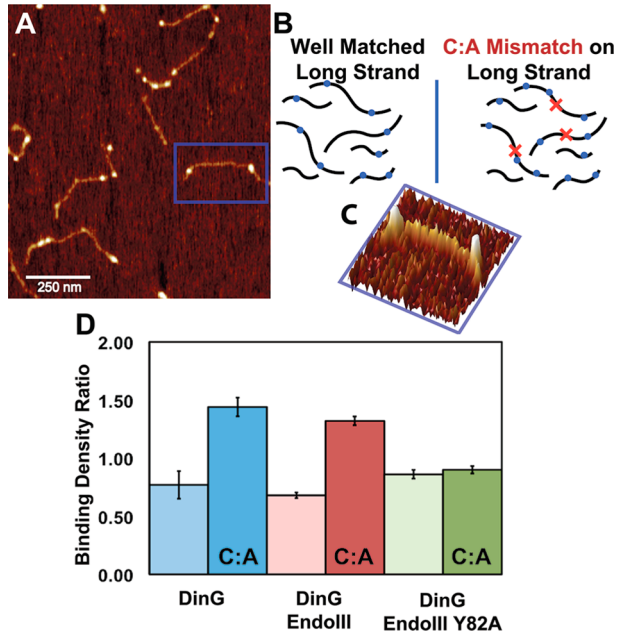

Figure 2. AFM redistribution assay. (A) A flattened image (Bruker nanoscope analysis software) for tapping-mode AFM topography of DinG-bound DNA adsorbed on mica. (B) Schematic representation of the redistribution assay. At equilibrium, repair proteins (blue) are preferentially localized on strands of DNA (black) with a C:A mismatch (red X). (C) Three-dimensional rendering of the blue-bordered region of the AFM image in A that shows a strand of DNA bound by two DinG proteins. (D) Measured binding density ratios, the density of proteins on long strands divided by the density of proteins on short strands, for proteins bound to mixtures of long and short strands of DNA with and without a mismatch (C:A) in the middle of the long strand. Three separate mixtures of protein and DNA were deposited onto individual surfaces, and at least 50 images were analyzed for each DinG (blue), a mixture of DinG and EndoIII (red), and a mixture of DinG and a CT-deficient mutant, Y82A EndoIII (green). ± SEM using a single image as a data point.

dx.doi.org/10.1021/ja501973c | J. Am. Chem. Soc. 2014, 136, 6470–6478

They share DNA sequence since the 3.8 kb strands are prepared by ligation of the two shorter strands.[22,35] For mixtures of mismatched long strands and well-matched short strands that are incubated with DinG alone, we find an average of 2.60 ± 0.22 proteins bound per mismatched strand compared to 0.90 ± 0.17 proteins per well-matched strand. We calculate the binding density on the mismatched and matched strands for each independent trial ($n \geq 3$ for each experiment) by normalizing the number of proteins bound by the strand length to obtain a binding density ratio of 1.44 ± 0.08 favoring the mismatched strand. Thus, even though DinG does not bind preferentially to a mismatch, DNA CT by DinG favors its redistribution onto the strand containing the single base mismatch.

Signaling between EndoIII and DinG was also tested by AFM. In 1:1 mixtures of DinG and wild-type (WT) EndoIII, a binding density ratio of 1.32 ± 0.04 favoring the mismatched strand is observed (Figure 2). But does this redistribution depend upon DNA CT? In 1:1 mixtures of DinG and EndoIII Y82A, a mutant protein that is defective in DNA-mediated CT,[22,35] a binding density ratio of 0.90 ± 0.03 is found (Figure 2); there is no preference for the mismatched strand (note that EndoIII does not bind preferentially to a mismatch).[22] This binding density ratio is comparable to what is observed for DinG alone when both strands are fully matched (Figure 2); when the proteins cannot carry out DNA CT, they cannot redistribute onto the strand containing the lesion. Since DinG can redistribute in the absence of EndoIII and DinG and EndoIII can redistribute when mixed only if EndoIII is effective in signaling by DNA CT, these observations support the need for effective signaling between EndoIII and DinG in finding the damaged strand. We have seen comparable results earlier in mixtures of SaXPD and EndoIII.[35]

It should be noted that protein loadings on the 3.8 kb strands are on the order of two proteins per strand under these experimental conditions. Therefore, assuming that DinG and EndoIII are signaling one another, for approximately half of the strands, signaling must occur between DinG and EndoIII rather than just between DinG partners or between EndoIII partners. Moreover, given a loading of about two proteins per strand, these results are consistent with DNA CT occurring over kilobase distances. It is also important to note that these proteins show no evidence of colocalizing at DNA sites by AFM. Overall, these data demonstrate that DinG and EndoIII can use DNA-mediated CT at long range to cooperate with one another to localize to regions of damage.

DinG Uses DNA-Mediated CT to Facilitate the Repair of DNA Damage by MutY. To begin to probe DNA-mediated signaling within the cell, a *lac*$^+$ forward reversion assay reporting on GC:TA transversions that reflects MutY activity within the CC104 strain of *E. coli* was utilized.[38] The CC104 strain reports on GC to TA transversions, which are prevented by MutY excising adenines improperly placed opposite an 8-oxodG lesion, in the lacZ gene. Cells in which this transversion process has occurred form colonies on plates containing lactose as the sole carbon source and are termed *lac*$^+$ revertants. Using this strain, changes in MutY activity can be assessed upon genetically knocking out DinG. If DinG and MutY cooperate in finding DNA lesions that attenuate CT, eliminating DinG from the cell should lead to a decrease in MutY activity and a corresponding increase in *lac*$^+$ revertants. We and others had earlier seen an effect of knocking out EndoIII on MutY activity in this assay.[22,41] When *dinG* is knocked out of the CC104 strain (CC104 Δ*dinG*), we find that the number of revertants increases 60% compared to WT CC104 (Table 1). While the effect is not high, it is notable given that knocking out MutY itself gives a maximum of 10−15 fold increase in revertant count under similar conditions.[22] It should also be noted that EndoIII and DinG do not have overlapping substrate specificity with MutY. A deletion of the *nth* gene from CC104 in combination with a deletion of the *mutY* gene resulted in the same number of revertants as that of the *mutY* deletion alone.[22] If the effect on MutY activity stems from lowering the concentration of DNA-bound 4Fe−4S proteins that cooperatively signal with MutY, then complementing the cells with a plasmid that expresses a mutant of EndoIII that contains a 4Fe−4S cluster, but is enzymatically inactive, p(EndoIII D138A) (Table 1),[22,42] should rescue MutY activity. Indeed, complementation with the plasmid for EndoIII D138A restores the activity of MutY in CC104 Δ*dinG*; the number of revertants found is comparable to WT CC104. However, complementing with a plasmid that expresses an EndoIII mutant, p(EndoIII Y82A), which is defective in DNA CT but nonetheless contains a 4Fe−4S cluster and is enzymatically active,[22] does not rescue MutY activity (Table 1). It should be noted that rescue with DinG was not explored, since overexpression of DinG using plasmids was previously observed to be toxic to cells.[33] While these data may not indicate dramatic effects, they are statistically significant and fully consistent with our model. These data thus suggest that MutY, EndoIII, and DinG may be capable of signaling one another via DNA-mediated CT to coordinate their activity in cells.

Table 1. MutY Activity Assay (CC104 *lac*$^+$ Forward Reversion Assay)

strain	plasmid[a]	no. of *lac*$^+$ revertants[b]	relative to CC104[c]
CC104	p(empty)	4.6 ± 0.4	1
CC104 Δ*dinG*	p(empty)	7.5 ± 0.7	1.6[d]
CC104	p(EndoIII D138A)	8.5 ± 1.1	1
CC104 Δ*dinG*	p(EndoIII D138A)	6.7 ± 0.6	0.8[d]
CC104	p(EndoIII Y82A)	3.4 ± 0.3	1
CC104 Δ*dinG*	p(EndoIII Y82A)	5.8 ± 0.8	1.7[d]

[a]See Table S2 for full plasmid designation. [b]Values for *lac*$^+$ revertants per 10^9 cells are reported for at least three independent trials ($N \geq 20$) ± SEM. [c]Relative to CC104 is defined as the ratio of *lac*$^+$ revertants for the CC104 *dinG* knockout strain to the number of *lac*$^+$ revertants for the wild-type CC104 strain containing the same plasmid as the CC104 *dinG* knockout strain [d]($p < 0.01$)

Repair of R-Loops by DinG Relies on DNA-Mediated Signaling by EndoIII in InvA. Perhaps more interesting to consider is the possibility of signaling in the reverse sense, with a BER protein signaling to DinG to aid DinG in finding its lesions, and here dramatic effects on survival are observed. Does EndoIII signaling aid DinG in locating R-loops, a substrate of DinG, in *E. coli*? R-loops are RNA:DNA hybrids that perturb duplex base stacking and would be expected to attenuate DNA CT, so that, based on the AFM results, DNA-mediated signaling could help DinG in its first step of finding its substrate. Here we took advantage of a strain, InvA, where the repair of R-loops by DinG is critical for cell survival. In the InvA strain, by inverting a frequently transcribed *rrnA* operon, the incidence of R-loop formation in cells is increased;[33] as a

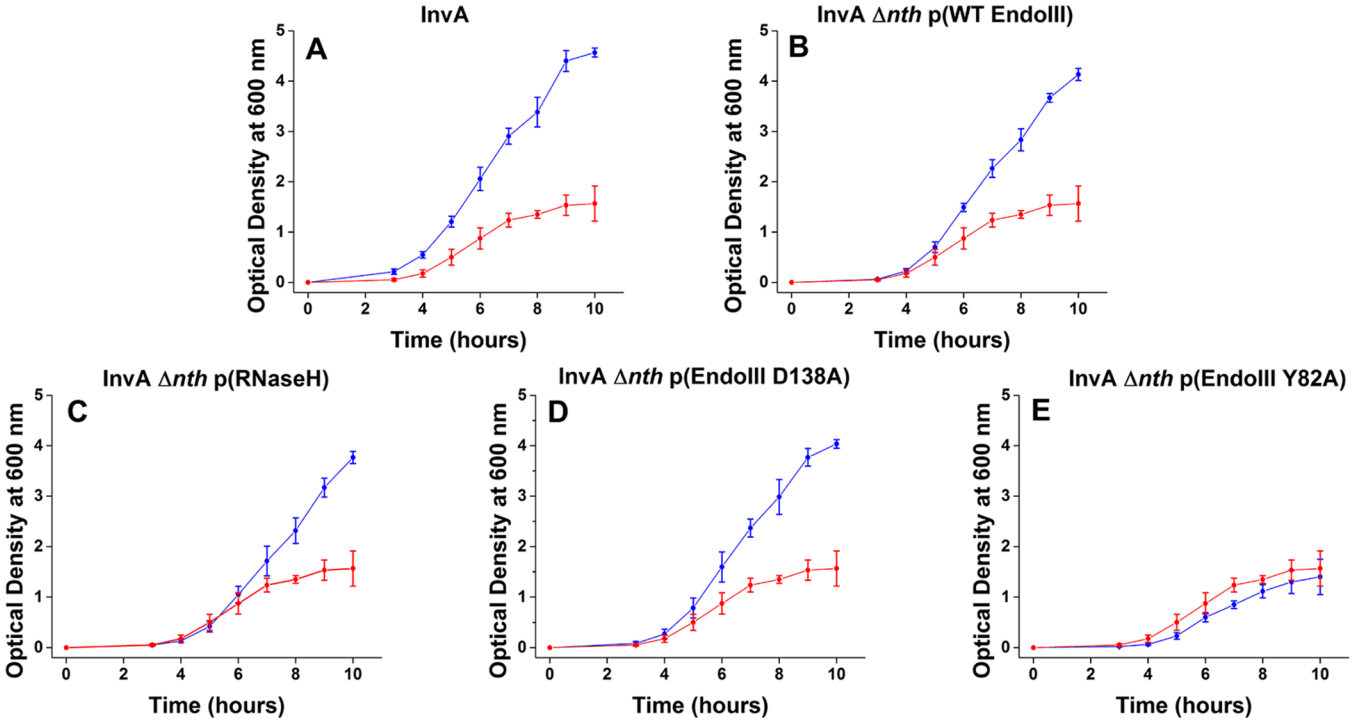

Figure 3. Rescue of growth defect conferred by knocking out *nth* in InvA. Cultures of LB were inoculated with single colonies of each strain and growth was monitored by optical density at 600 nm over time. Strains of InvA Δ*nth* grew comparably to InvA Δ*nth* transformed with p(empty) showing that the effect is not due to the presence of the plasmid. Data were recorded for at least three independent trials. (A) Growth of InvA WT (blue) or InvA Δ*nth* transformed with p(empty) (red) ± SEM. (B) Growth of InvA Δ*nth* transformed with p(WT EndoIII) (blue) or p(empty) (red) ± SEM. (C) Growth of InvA Δ*nth* transformed with p(RNaseH) (blue) or p(empty) (red) ± SEM. (D) Growth of InvA Δ*nth* transformed with p(EndoIII D138A) (blue) or p(empty) (red) ± SEM. (E) Growth of InvA Δ*nth* transformed with p(EndoIII Y82A) (black) or p(empty) (red) ± SEM.

result, replication forks stalling, when they collide head-on with the transcription machinery, are necessarily amplified in the InvA strain. Resolving stalled replication forks is vital to preventing significantly deleterious DNA damage and thus to survival.[33,43] In previous work it has been shown that within the InvA strain, the repair of R-loops by DinG was shown to be essential to maintain viability; deletion of *dinG* yielded a significant plating defect.[33] Rescue by overexpression of RNaseH is a hallmark of R-loop-dependent phenotypes, as RNaseH endonucleolytically degrades RNA within an RNA:DNA hybrid but not free RNA.[33] Complementing the InvA Δ*dinG* strain with a plasmid encoding RNaseH thus rescued activity.[33] Growth assays to test DinG activity using InvA are particularly advantageous in testing signaling with other proteins since the growth defect is dramatic; knocking out signaling partners should similarly yield clearly discernible effects.

To test signaling between EndoIII and DinG, we prepared an EndoIII knockout in the InvA strain (InvA Δ*nth*). If signaling with EndoIII is essential for DinG to effectively repair R-loops, consistent with our model, we would expect to observe effects on cell viability upon knocking out the *nth* gene in InvA. After incubation in LB for several hours, growth of the InvA Δ*nth* strain is indeed compromised compared to the InvA parent strain (Figure 3). If the strains are instead grown under nutrient deprivation in minimal media, cellular viability is completely lost (Figure S3). The growth curves for InvA Δ*nth* alongside InvA or InvA Δ*nth* strains with transformed plasmids that express various EndoIII mutants and RNaseH are shown in Figure 3. If the growth defect for InvA Δ*nth* is the result of the ineffective repair of R-loops, as was seen for the InvA Δ*dinG* phenotype, complementation with a plasmid that overexpresses RNaseH, p(RNaseH), should restore activity, which is observed. This result indicates signaling between EndoIII and DinG but does not elucidate the mechanism of signaling. The cooperative signaling effect is not due to the enzymatic activity of EndoIII. The p(EndoIII D138A) plasmid, which expresses the EndoIII mutant lacking glycosylase activity but containing a 4Fe−4S cluster, also rescues the InvA Δ*nth* strain. But is this cooperative signaling the result of long-range DNA CT among 4Fe−4S proteins? While expressing WT EndoIII restores activity in InvA Δ*nth*, complementation with the CT-defective, but enzymatically proficient p(EndoIII Y82A) plasmid does not. These results strongly correlate with the results from the AFM and reversion assays, and it appears that EndoIII signals to DinG via DNA CT to help DinG locate and process R-loops.

DISCUSSION

Our model for how DNA repair proteins with 4Fe−4S clusters use DNA-mediated CT as a first step in locating lesions to repair is depicted in Figure 4. Critical to the model is the fact that the DNA binding affinity of a protein that has a 4Fe−4S cluster is dependent on the oxidation state of the cluster. For these proteins, the shift in reduction potential upon DNA binding necessitates a lower DNA binding affinity of at least 3 orders of magnitude for a 200 mV shift when in the reduced form (2+) compared to the oxidized form (3+).[19] Figure 1 shows that the DNA-bound potential is significantly shifted from that reported in the absence of DNA.[30] Therefore, as illustrated in Figure 4, 4Fe−4S clusters in these proteins when

dx.doi.org/10.1021/ja501973c | J. Am. Chem. Soc. 2014, 136, 6470−6478

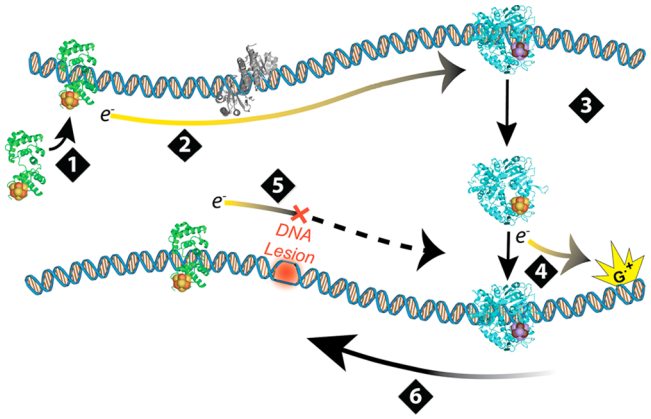

Figure 4. Scheme depicting how repair proteins may use DNA-mediated signaling to search for damage. The model describes how DNA CT can drive the redistribution of the repair proteins into the vicinity of damage. (1) A protein with a reduced (orange-yellow) iron–sulfur cluster binds to DNA. (2) This protein's iron–sulfur cluster is oxidized (purple-brown) by another DNA-bound redox-active protein. This oxidation can occur over long distances and through other DNA-bound proteins (gray) so long as the π-orbital stacking of bases between the reductant and oxidant is unperturbed. (3) Reduction promotes the repair protein's dissociation from DNA. (4) The repair protein binds to an alternate DNA site where it is oxidized either by a guanine radical or another protein. (5) DNA lesions between proteins inhibit electron transport, so protein dissociation is not promoted. (6) Proteins that are now in close proximity to the lesion are able to move processively toward the damage for repair.

they are freely diffusing are expected to be in the 2+ state. Upon binding to DNA, however, the proteins are activated towards oxidation. A given protein already bound to DNA in the oxidized form, perhaps oxidized from a distance by a guanine radical generated under oxidative stress,[44] could thus be reduced in a DNA-mediated fashion by another distinct redox-active protein that binds within CT distance of the first protein. Reducing this second protein would promote its dissociation from DNA. This interprotein signaling requires an undamaged path between the two proteins; intervening DNA damage prevents the protein from receiving reducing equivalents so that its dissociation is not promoted. Effectively, this electron-transfer event signals the repair protein to dissociate from undamaged regions and search for damage elsewhere in the genome. If there is an intervening damage product that blocks CT, however, then the repair protein stays bound in the vicinity of damage, and the protein can move on a slower time scale to the local site in need of repair. This process would lead to the redistribution of repair proteins in the vicinity of damage through an efficient scanning of the genome by proteins of similar redox potential. In essence, these proteins inform one another about the integrity of DNA by using DNA as a medium through which they transmit electronically encoded information. Because this signaling occurs over long distances, this mechanism would significantly reduce the time required to scan the genome, allowing for enzymes to repair the genome on biological time scales. Indeed, even when CT distances of only 100 bases, that which we have documented, are permitted in our model, a significant reduction in search time to scan the *E. coli* genome can be predicted.[22] Importantly, other models have been investigated for how BER enzymes similar to MutY and EndoIII can scan the genome and locate their substrates. For example, it has been shown that one-dimensional sliding along DNA can be fast enough for glycosylases to come into contact with bases in the genome on the order of seconds.[45a−c] Models for one-dimensional sliding do not, however, take into account protein traffic along the genome. It is important to note that DNA-mediated CT is not interrupted by intervening bound proteins as long as the proteins do not perturb the base pair stack. Thus, sliding, hopping, and DNA CT models taken together offer an appealing means to explain how the search process may be optimized under the realistic conditions of the cell.

Data from DNA-modified electrochemistry experiments show that the DNA-bound reduction potential of DinG is remarkably similar to that for EndoIII, MutY, and SaXPD.[19−21] As such, DinG is competent to shuttle electrons through DNA to or from EndoIII or MutY via its 4Fe−4S cluster, as would be required by the model proposed for the redistribution of these proteins to sites of damage. As with EndoIII and MutY, we consider the redox potential of DinG to correspond to the $[4Fe{-}4S]^{3+/2+}$ couple that is now accessible due to the negative potential shift associated with binding to the DNA polyanion.[19] The ATP-dependent increase in current intensity observed for DinG on electrodes is consistent with previous results for SaXPD, except that the signal increase is nearly an order of magnitude higher than that observed for the thermophilic SaXPD.[21] This substantial difference in signal increase is understandable based upon the significantly lower rate of ATP hydrolysis of SaXPD versus DinG at ambient temperature. It is interesting to consider that the increase in signal intensity could be a general characteristic of these DNA enzymes that contain redox-active clusters, where they signal not only their presence but also their activity. For DinG, there could be signaling to upstream proteins that DinG is in the process of unwinding its substrate.

The AFM experiments, moreover, support signaling between EndoIII and DinG *in vitro*. Based on the model, we expect the redistribution of proteins that use DNA-mediated CT signaling onto strands containing a single base mismatch and away from fully matched duplex DNA, which is the observed result. Proteins that are defective in DNA CT, furthermore, do not relocate to the mismatched strand, as predicted by our model. Since R-loops disrupt DNA CT, it would be expected that this chemistry could be used within a cell as a first step to drive the redistribution of DinG into the vicinity of R-loops as well; a binding preference of DinG for the R-loop would lead to subsequent localization.

Importantly, the genetics experiments point to a role for DNA-mediated signaling by DinG and other proteins with 4Fe−4S clusters within the cell. Based on the hypothesis that any DNA processing enzymes with 4Fe−4S clusters of similar potential can cooperate, we would expect signaling between EndoIII and DinG and also signaling between MutY and DinG. The *lac*$^+$ forward reversion assay demonstrates that DinG does indeed help MutY find and process its substrate, since knocking out DinG results in an increase in mutagenesis associated with a decrease in MutY activity. Moreover, expressing an enzymatically deficient mutant of EndoIII still rescues activity, while a CT-deficient mutant does not. Interestingly, this mutagenesis is suppressed by expression of EndoIII, despite the fact that EndoIII does not repair the same lesions as MutY.[22] It is remarkable to consider that an effect caused by knocking out a helicase can be reversed by expressing a separate DNA glycosylase, EndoIII. What they have in common is the 4Fe−

dx.doi.org/10.1021/ja501973c | J. Am. Chem. Soc. 2014, 136, 6470−6478

4S cluster. These results provide genetic evidence that the effect of knocking out DinG is due to DinG aiding MutY in processing its target lesion via DNA-mediated CT.

It is critical in the context of this model to demonstrate not only that DinG affects the activity of base excision repair enzymes with 4Fe−4S clusters but also that base excision repair enzymes affect the activity of DinG. Within the InvA strain, R-loop formation is significantly amplified, and the repair of R-loops becomes essential for cell viability under certain conditions. The fact that DinG is critically important in the InvA strain is understandable. But we find that by knocking out even EndoIII in InvA, a dramatic growth defect in LB and a complete loss of cellular viability under low nutrient conditions is observed. Since RNaseH can compensate for a loss of DinG activity by degrading R-loops, overexpression of RNaseH restoring normal growth confirms that the observed growth defect is due to EndoIII aiding DinG in processing R-loops. Just as was seen in the *lac*$^+$ forward reversion assay, expression of the enzymatically inactive but CT-proficient EndoIII D138A can also restore normal growth. Expressing EndoIII Y82A, which is CT-deficient, however, does not rescue growth. Therefore, it is not the loss of glycolytic activity of EndoIII that is suppressing growth in an EndoIII knockout in InvA but the loss of the ability of EndoIII to carry out DNA-mediated CT chemistry.

Overall these results provide substantial evidence, using both AFM and genetics experiments, that *E. coli* enzymes from distinct repair pathways signal one another from a distance through DNA as long as the proteins remain competent to carry out DNA-mediated CT, as measured electrochemically. The AFM experiments show that a single base mismatch in a 3.8 kb duplex is sufficient to promote the redistribution of the 4Fe−4S proteins to damaged DNA, driven by long-range signaling. The genetics experiments emphasize that cooperative signaling for repair within the cell requires the ability of the proteins with 4Fe−4S clusters to carry out DNA CT, not their primary enzymatic activity. Signaling through DNA CT is fast (ps),[46] can occur over long molecular distances, and allows for the binding of many intervening proteins, as long as their distortion of the DNA duplex is minimal. As such, DNA CT provides a mechanism for efficient signal transduction on biological time scales, as the cell requires. Our proposed redistribution model is one way in which proteins may use DNA CT to efficiently scan the genome as a first step in finding lesions to repair and to prepare the genome for replication. The utilization of DNA CT by enzymes to maintain cellular viability and genomic integrity represents a novel role for 4Fe−4S clusters in DNA processing enzymes. A growing body of evidence is emerging that highlights the importance of iron−sulfur clusters in enzymes that are involved in nearly every aspect of DNA metabolism. The results here provide a basis for understanding the ubiquity of 4Fe−4S clusters in proteins that maintain the integrity of the genome throughout the phylogeny.

■ ASSOCIATED CONTENT

Supporting Information

Experimental analysis and supporting figures and tables. This material is available free of charge via the Internet at http://pubs.acs.org.

■ AUTHOR INFORMATION

Corresponding Author

jkbarton@caltech.edu

Notes

The authors declare no competing financial interest.

■ ACKNOWLEDGMENTS

We are grateful to the NIH (GM49216), the Moore Foundation (Caltech Signaling Center), and the Center for Environmental Microbial Interactions (CEMI, Caltech) for their financial support. M.A.G. and H.M.S. were NIH predoctoral trainees (NIH/NRSA 5T32GM07616) and T.J.Z. an NSF fellow (DGE-1144469). We are also grateful to the Beckman Institute MMRC for AFM instrumentation. We thank Dr. Huangen Ding (Louisiana State University, Baton Rouge, LA) for helpful discussions regarding DinG, the Coli Genetic Stock Center (CGSC, Yale) for distributing the BW16847 and JW1625-1, and Dr. B. Michel (Gif-sur-Yvette) for the gift of the InvA bacterial strain and RNaseH overexpression plasmid. Lastly we thank Ms. Janani Comar for research assistance.

■ REFERENCES

(1) Genereux, J. C.; Boal, A. K.; Barton, J. K. *J. Am. Chem. Soc.* **2010**, *132*, 891.

(2) Wu, Y.; Brosh, R. M., Jr. *Nucleic Acids Res.* **2012**, *40*, 4247.

(3) White, M. F.; Dillingham, M. S. *Curr. Opin. Struct. Biol.* **2012**, *22*, 94.

(4) Cunningham, R. P.; Asahara, H.; Bank, J. F.; Scholes, C. P.; Salerno, J. C.; Surerus, K.; Munck, E.; McCracken, J.; Peisach, J.; Emptage, M. H. *Biochemistry* **1989**, *28*, 4450.

(5) Wu, Y.; Suhasini, A. N.; Brosh, R. M., Jr. *Cell. Mol. Life Sci.* **2009**, *66*, 1209.

(6) Weiner, B. E.; Huang, H.; Dattilo, B. M.; Nilges, M. J.; Fanning, E.; Chazin, W. J. *J. Biol. Chem.* **2007**, *282*, 33444.

(7) Netz, D. J. A.; Stith, C. M.; Stümpfig, M.; Köpf, G.; Vogel, D.; Genau, H. M.; Stodola, J. L.; Lill, R.; Burgers, P. M. J.; Pierik, A. J. *Nat. Chem. Biol.* **2011**, *8*, 125.

(8) Yeeles, J. T. P.; Cammack, R.; Dillingham, M. S. *J. Biol. Chem.* **2009**, *284*, 7746.

(9) Saikrishnan, K.; Yeeles, J. T.; Gilhooly, N. S.; Krajewski, W. W.; Dillingham, M. S.; Wigley, D. B. *EMBO J.* **2012**, *31*, 1568.

(10) Pokharel, S.; Campbell, J. L. *Nucleic Acids Res.* **2012**, *40*, 7821.

(11) Liu, H.; Rudolf, J.; Johnson, K. A.; McMahon, S. A.; Oke, M.; Carter, L.; McRobbie, A. M.; Brown, S. E.; Naismith, J. H.; White, M. F. *Cell* **2008**, *133*, 801.

(12) Fan, L.; Fuss, J. O.; Cheng, Q. J.; Arvai, A. S.; Hammel, M.; Roberts, V. A.; Cooper, P. K.; Tainer, J. A. *Cell* **2008**, *133*, 789.

(13) Wolski, S. C.; Kuper, J.; Haenzelmann, P.; Truglio, J. J.; Croteau, D. L.; Van-Houten, B.; Kisker, C. *PLoS Biol.* **2008**, *6*, 1332.

(14) Porello, S. L.; Cannon, M. J.; David, S. S. *Biochemistry* **1998**, *37*, 6465.

(15) Veatch, J. R.; McMurray, M. A.; Nelson, Z. W.; Gottschling, D. E. *Cell* **2009**, *137*, 1247.

(16) Stehling, O.; Vashisht, A. A.; Mascarenhas, J.; Jonsson, Z. O.; Sharma, T.; Netz, D. J. A.; Pierik, A. J.; Wohlschlegel, J. A.; Lill, R. *Science* **2012**, *337*, 195.

(17) Gari, K.; Léon Ortiz, A. M.; Borel, V.; Flynn, H.; Skehel, J. M.; Boulton, S. J. *Science* **2012**, *337*, 243.

(18) Sontz, P. A.; Muren, N. B.; Barton, J. K. *Acc. Chem. Res.* **2012**, *45*, 1792.

(19) Gorodetsky, A. A.; Boal, A. K.; Barton, J. K. *J. Am. Chem. Soc.* **2006**, *128*, 12082.

(20) Boal, A. K.; Yavin, E.; Lukianova, O. A.; O' Shea, V. L.; David, S. S.; Barton, J. K. *Biochemistry* **2005**, *44*, 8397.

(21) Mui, T. P.; Fuss, J. O.; Ishida, J. P.; Tainer, J. A.; Barton, J. K. *J. Am. Chem. Soc.* **2011**, *133*, 16378.

(22) Boal, A. K.; Genereux, J. C.; Sontz, P. A.; Gralnick, J. A.; Newman, D. K.; Barton, J. K. *Proc. Natl. Acad. Sci. U.S.A.* **2009**, *106*, 15237.
(23) Genereux, J. C.; Barton, J. K. *Chem. Rev.* **2010**, *110*, 1642.
(24) Boal, A. K.; Barton, J. K. *Bioconj. Chem.* **2005**, *16*, 312.
(25) Boon, E. M.; Salas, J. E.; Barton, J. K. *Nat. Biotechnol.* **2002**, *20*, 282.
(26) Kelley, S. O.; Jackson, N. M.; Hill, M. G.; Barton, J. K. *Angew. Chem., Int. Ed.* **1999**, *38*, 941.
(27) Gorodetsky, A. A.; Buzzeo, M. C.; Barton, J. K. *Bioconj. Chem.* **2008**, *19*, 2285.
(28) Núñez, M. E.; Hall, D. B.; Barton, J. K. *Chem. Biol.* **1999**, *6*, 85.
(29) Slinker, J. D.; Muren, N. B.; Renfrew, S. E.; Barton, J. K. *Nat. Chem.* **2011**, *3*, 228.
(30) Ren, B.; Duan, X.; Ding, H. *J. Biol. Chem.* **2009**, *284*, 4829.
(31) Voloshin, O. N.; Vanevski, F.; Khil, P. P.; Camerini-Otero, R. D. *J. Biol. Chem.* **2003**, *278*, 28284.
(32) Voloshin, O. N.; Camerini-Otero, R. D. *J. Biol. Chem.* **2007**, *282*, 18437.
(33) Boubakri, H.; Langlois de Septenville, A.; Viguera, E.; Michel, B. *EMBO J.* **2010**, *29*, 145.
(34) Pheeney, C. G.; Arnold, A. R.; Grodick, M. A.; Barton, J. K. *J. Am. Chem. Soc.* **2013**, *135*, 11869.
(35) Sontz, P. A.; Mui, T. P.; Fuss, J. O.; Tainer, J. A.; Barton, J. K. *Proc. Natl. Acad. Sci. U.S.A.* **2012**, *109*, 1856.
(36) Datsenko, K. A.; Wanner, B. L. *Proc. Natl. Acad. Sci. U.S.A.* **2000**, *97*, 6640.
(37) Kovach, M. E.; Elzer, P. H.; Hill, D. S.; Robertson, G. T.; Farris, M. A.; Roop, R. M., II.; Peterson, K. M. *Gene* **1995**, *166*, 175.
(38) Cupples, C. G.; Miller, J. H. *Proc. Natl. Acad. Sci. U.S.A.* **1989**, *86*, 5345.
(39) Thomason, L.; Constantino, N.; Court, D. L. *Curr. Protoc. Mol. Biol.* **2007**, *79*, 10.5.1−10.5.11.
(40) Miller, J. H. *A Short Course in Bacterial Genetics*; Cold Spring Harbor Laboratory Press: Cold Spring Harbor, NY, 1992.
(41) Tano, K.; Iwamatsu, Y.; Yasuhira, S.; Utsumi, H.; Takimoto, K. *J. Radiat. Res.* **2001**, *42*, 409.
(42) Thayer, M. M.; Ahern, H.; Xing, D.; Cunningham, R. P.; Tainer, J. A. *EMBO J.* **1995**, *14*, 4108.
(43) Aguilera, A.; García-Muse, T. *Mol. Cell* **2012**, *46*, 115.
(44) Yavin, E.; Boal, A. K.; Stemp, E. D. A.; Boon, E. M.; Livingston, A. L.; O'Shea, V. L.; David, S. S.; Barton, J. K. *Proc. Natl. Acad. Sci. U.S.A.* **2005**, *102*, 3546−3551.
(45) (a) Blainey, P. C.; van Oijen, A. M.; Banerjee, A.; Verdine, G. L.; Xie, X. S. *Proc. Natl. Acad. Sci. U.S.A.* **2006**, *103*, 5752. (b) Dunn, A. R.; Kad, N. M.; Nelson, S. R.; Warshaw, D. M.; Wallace, S. S. *Nucleic Acids Res.* **2011**, *39*, 7487. (c) Wallace, S. S. *Environ. Mol. Mutagen.* **2013**, *54*, 691.
(46) Wan, C.; Fiebig, T.; Kelley, S. O.; Treadway, C. R.; Barton, J. K.; Zewail, A. H. *Proc. Natl. Acad. Sci. U.S.A.* **1999**, *96*, 6014.